An Experimental Analysis of the Structural Response of Flexible Lightweight Hydrofoils in Various Flow Conditions

Alexandra Lelong, Pierre Guiffant, Jacques André Astolfi

An Experimental Analysis of the Structural Response of Flexible Lightweight Hydrofoils in Various Flow Conditions

Alexandra Lelong[1],Pierre Guiffant[1], Jacques André Astolfi[1]*

ISROMAC 2016

International Symposium on Transport Phenomena and Dynamics of Rotating Machinery

Hawaii, Honolulu

April 10-15, 2016

Abstract

The paper presents the results of an experimental study of the hydroelastic response of flexible lightweight hydrofoils undergoing various flow conditions including unsteady partial cavitating flow. It is based on the analysis of the static deformation, the vibrations, the strains and the stresses of cantilevered hydrofoils, at Reynolds number ranging from 3.10^5 to 6.10^5 in a hydrodynamic tunnel. A specific distance measurement laser device was used to measure the static deformation of the hydrofoil for bending and twisting. The vibration response was measured by means of two laser vibrometers in order to identify the modal response, mainly the first bending and twisting modes. The strains and stresses were obtained from integrated strain gauges imbedded in the foil close to the root section. A high speed camera was used in order to analyze unsteady features of the cavitating flow in some cases. The paper presents the experimental setup and the main results are discussed.

Keywords

flexible hydrofoil — cavitation — hydroelastic response — strains — vibration — modal analysis

[1]*Department of Mechanical Engineering, Naval Academy Research Institute, Lanvéoc-Poulmic, France*

***Corresponding author**: jacques-andre.astolfi@ecole-navale.fr

INTRODUCTION

In hydraulic rotating machines, the perspective of using lightweight structures with a certain degree of flexibility is a challenging way to reduce the weight, to enhance the performance and opens possibility to control the machine. For instance an improvement can come from the use of flexible lifting structures that could adapt passively or actively to variable operating conditions. However using flexible lightweight structural in water gives rise to basic questions related to Fluid Structure Interaction in a high density fluid that is quite different from aeroelasticity for which the fluid density is much smaller than the mean structure density in many applications as aerospace or wind engineering. For hydraulic rotative machine operating at relative high velocity, structures are subjected to high loadings due to the high density of water and relative large velocity. Using nonmetallic and lighter materials can lead to high stresses and significant deformation inducing strong coupling with the flow. Moreover from a dynamical point of view, several points need to be well understood as the dynamic structural response related to added-mass effects, damping, stiffness together with possible flow-structure instabilities in turbulent high Reynolds and potentially cavitating flows. The latter is of primary importance for hydraulic machine design . The control of cavitation occurring as the minimum pressure in the fluid is lower than the vapor pressure ([1], [2])is a very challenging task and using active or passive flexible structures is a way that should be of great interest. In hydraulic machine, operating flow conditions induce strong low pressure on the suction side of blades leading to various kinds of cavitation according to the angle of attack ([3]). For instance, it is known that for small angles of incidence, travelling bubble occur on the suction side and that leading edge cavitation (namely partial or sheet cavitation) occurs for larger angles of incidence. Moreover under specific conditions, the vaporized area becomes unstable, with cavity break-off and periodical shedding of large bubble clusters. This configuration, named "cloud cavitation", generates pressure fluctuations downstream of the cavity that was studied largely on rigid structures ([4]) but is unknown when coupling with flexible structures. Recent efforts were made in order to approach through simulations both the fluid and the structure dynamics. This comes from the recent development of numerical methods and models which allow to compute complex flows together with coupled simulation with reasonable CPU time, (see [5]). Some numerical developments were developed to analyze fluid-structure interaction (FSI) of flexible composite structure in hydraulic applications mainly for marine propellers ([6], [7], [8], [5], [9], [10], [11]). However the numerical developments suffer from a lack of experimental data. For instance, although a large

number of experimental studies deals with the analysis of cavitation over rigid hydrofoils ([4],[12]) little referred to experimental cavitation on flexible structures. Ausoni at al. ([13]) studied experimentally the vibration response of a metallic hydrofoil but only recently, cavitation over a flexible hydrofoil has been studied numerically and experimentally ([14], [15], [16],[17], [18] and [19]) or theoretically ([20], [21]). Theses studies deal with the vibration induced by the cavitation on a 3D hydrofoil or a two degrees of freedom model of a rigid hydrofoil in pitching and heaving motion. They indicated that cavitation can change the modal response of the structure and that a lock-in of the foil's frequencies in cavitating flows can occur in specific conditions but that experimental data and physical observations are still required for a better understanding of a complex FSI phenomena to be beneficial for simulation of FSI in hydraulic applications.

The present paper deals with a collaborative research program between the French Naval Academy and the Department of Naval Architecture and Marine Engineering at the University of Michigan in order to analyze the hydroelastic response of a flexible homogeneous hydrofoil in various flow conditions including cavitating flow. The objective of the program is to perform physical analysis as well as to improve simulations of FSI for heavy fluid applications.

1. EXPERIMENTAL SETUP

The experiments were carried out in the cavitation tunnel of Naval Academy Research Institute (IRENav) fitted with a 192 mm square test section of 1m long (Figure 1). The flow velocity ranges between 3 and 12m.s-1 and the pressure in the tunnel test section is between 3 bars to 100 mbar mainly to control cavitation inception. The inlet turbulence intensity measured about two chords from the hydrofoil leading edge by LDV is close to 2%.

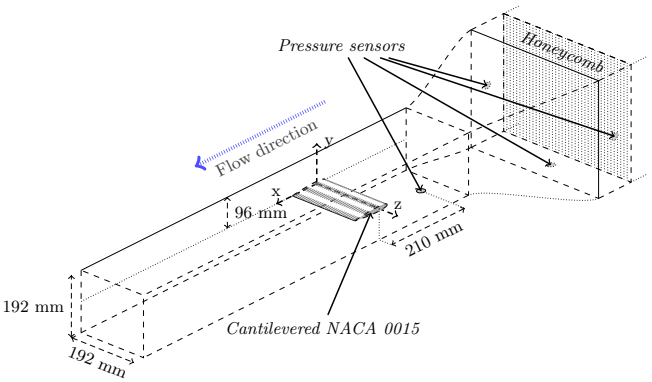

Figure 1. Cavitation tunnel of IRENav.

Two NACA 0015 flexible foils of c = 100mm chord and b = 191mm span were used. The first one was used for strain and vibration measurements. It was constituted of a cylindrical base that insure a quasi-perfect clamped condition at the foil root forming a cantilevered flexible hydrofoil. It was set into a cylindrical rigid aluminium base (Figure 2). The foil was obtained by milling a Polyoxymethylene plastic (POM, Table 1). The other foil was used to measure static deformation. In that case, the flexible part was fabricated using stereolithography 3D printing using POLY1500 resin. In both case the rotation axis was located at x/c = 0.5 from the leading edge. The characteristics of the material are given in the Table 1 and compared with the steel's ones for information.Note the uncertainties on the POLY1500 resin.

Figure 2. Cantilevered flexible hydrofoil equipped with strain gauges at the root

The incidence of the foil in the tunnel is controlled by a Baldor drive system that allows us to control with high accuracy the angle step $\Delta\alpha$, the acceleration and the rotational speed. The theoretical accuracy of the adjustment is 6.10^{-4} degree, however the uncertainties of the angle of attack was founded to be 0.1°, considering the mechanical mounting system. A high speed camera was fixed over the test section to record movies when cavitation develops over the foil. The model used is a Fastcam SA3 120K from Photron. It is equipped with a CMOS image sensor, which sensor size is 17.4mm*17.4mm. The frame rate is spread from 60fps to 2000fps for the full sensor resolution (1024*1024 pixels), when the pixel size is 17μm.

Table 1. Characteristics of the flexible materials. Steel is given for comparison.

	Steel	POM	POLY1500
Young mod. (E, GPa)	203	2.9	1.227–1.462
Poisson coef. (ν)	0.30	0.35	—-
Density (ρ, kg.m^{-3})	8010	1420	1180 – 12000

1.1 Static deformation measurements

The static deformation was measured using a Laser distance measurement system mounted on a 2D translation system on the uper side of the test section. The system

allowed us to scan the hydrofoil surface for a given flow condition along various sections selected along the span. In that case five sections from the root to the tip was selected. Then the deformation was obtained by comparing the scan without flow and the scan obtained at a given velocity. With this method it was possible to extract the bending and twisting of the hydrofoil for a given angle of incidence and velocity. However, a specific geometrical system was used to calibrate the laser distance measurement in order to take into account of the deflection of the beam laser crossing the Plexiglas and the water layers. The calibration consisted to measure the position of a well-known geometrical system in air then to measure the same system position with water and Plexiglas layers. A correction factor was then found in such a way the two mesaurements give the same results. The correction factors were aplied to the measurements.The results are presented on Figure 3 for the static bending at mid-chord and on Figure 4 for twisting. As shown the hydrofoil experienced mostly bending ranging from 1mm to 10mm than twisting ranging within 0.05° and 0.1° according the angle of incidence.

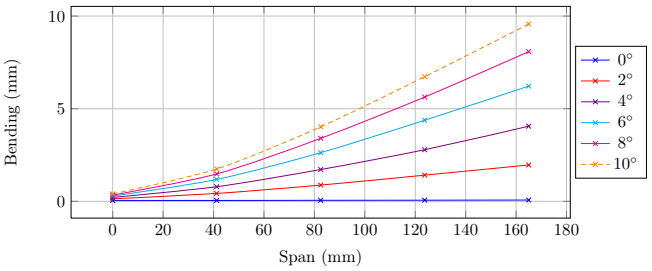

Figure 3. Deformation of the POLY1500 hydrofoil with $U = 5\text{m.s}^{-1}$ - bending.

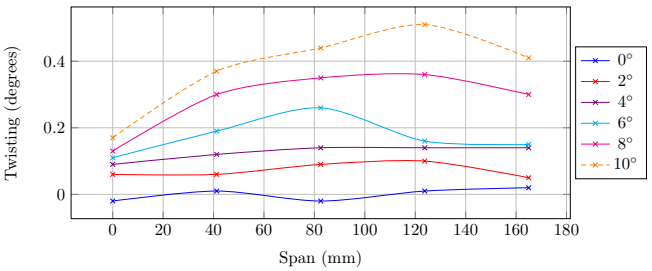

Figure 4. Deformation of the POLY1500 hydrofoil with $U = 5\text{m.s}^{-1}$ - twisting.

1.2 Strain measurements

To determine components of plane strain, the hydrofoil is equipped with three identical strain gauges build in a rosette way. They are glued in a hole close to the root of the foil. The cavity is filled with a resin whose mechanical characteristics are close to the foil's material. The cavity is then polished with sand paper to obtain a smooth continuous surface (Figure 2).

The strain gauges are L2A_13-125WW-120 from Vishay Micro Measurements. They are made in constantan and have a K-factor equal to 2.11. Their accuracy is ±6%. The strain gauges are assembled in a Quarter Bridge . The strain gauges measure the strains ($\varepsilon_{1,2,3}$ in the direction of their own axis. The gauges' axes are separated by a 45° angle and the first one is given by the span direction (ε_1), the third by the chord direction ((ε_3). The data are first amplified (Quantum mx16, HBM) and then recorded by the acquisition software CATMAN (HBM).

The principal strains $\varepsilon_{I,II}$ can be calculated by:

$$\varepsilon_{I,II} = \frac{\varepsilon_1 + \varepsilon_3}{2} \pm \frac{1}{2}\sqrt{(\varepsilon_3 - \varepsilon_1)^2 + 4 * (\varepsilon_2 - \frac{1}{2}(\varepsilon_1 + \varepsilon_3))^2} \tag{1}$$

as well as the principal stresses $\sigma_{I,II}$:

$$\sigma_{I,II} = \lambda(\varepsilon_I + \varepsilon_{II}) + 2\mu\varepsilon_{I,II} \tag{2}$$

with $\lambda = \frac{E\nu}{(1+\nu)(1-2\nu)}$ and $\mu = \frac{E}{2(1+\nu)}$ the Lamé parameters.

The Von Mises stress can be computed as well by:

$$\sigma_{VM} = \sqrt{\sigma_I^2 + \sigma_{II}^2 - \sigma_I\sigma_{II}} \tag{3}$$

1.3 Vibration measurements

The measurements were performed with two vibrometers from Polytec: the first one is fixed and is taken as a reference whereas the second one is a PSV-400 scanning vibrometer. This model can detect vibrations up to 10m.s^{-1} with a HeNe laser ($\lambda = 633$nm). It is equipped with two analog velocity decoder VD-04 and VD-06. The scanner is a high precision scan unit, with an angular resolution lower than 0.002° and an angular stability lower than 0.01° per hour. Because of laser light diffusion in the platic material, reflecting tapes were glued on the foil's surface to enhance the signal to noise ratio. It allows us to measure the vibration level on a user-defined grid over the structure surface. The cross-spectrum between the reference laser point and a scanned measured point is computed to preserve the phase at a given frequency. From this phase, the phase between two scanned points measured at two different time could be computed. This allowed us to get the vibration shape of the structure at a given frequency. It is very convenient to infer the modal shape associated to a modal frequency.

An electrodynamic shaker was used to measure the response of the foil to an impulse and identify the natural frequencies of the foil in air and in still water. Eight measurements were performed on each point, with one impulse per measurement, and the mean spectrum was calculated. The frequency resolution of the following measurements is $\Delta f = 0.625$Hz. The repeatability of the experiment was tested and the accuracy was then lower than 2%.

The modes have been identified thanks to the phase preservation between the reference and the scanning vibrometer. The spectra are shown on figure 5 and the values of the three first modes' frequencies are given in Table 2. As shown, the frequencies of the bending (f_1) and twisting (f_2) modes in water decrease strongly compared to in the air as a result of added mass effects. The modal shapes are given on Figures 6(a) and 6(b) for bending and twisting. The mean bending and twisting along the chord for various sections is compared to a beam theoretical bending and twsting modes showing that the 3D hydrofoil has a beam like behavior for the two first modes of vibration (Figures 7 and 8)

Table 2. First modes' frequencies of the foil in POM as response to series of eight impulses (Hz).

	Air	Still water
f_1	80.6	34.4
f_2	390	183.5
f_3	556.5	292

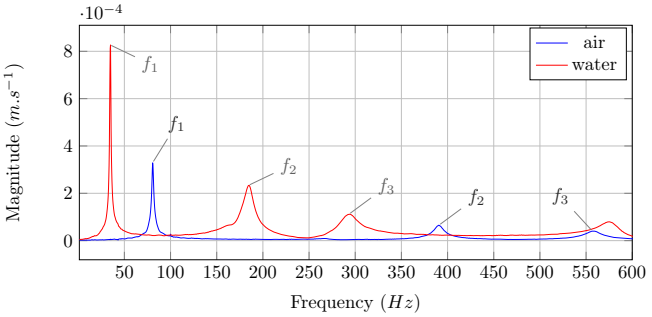

Figure 5. Response of the foil in POM to an impulse in $\mathrm{m.s^{-1}}$.

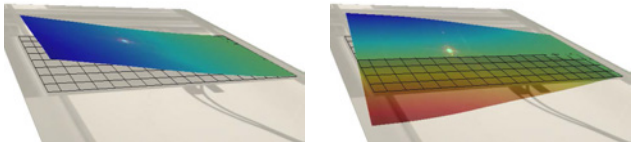

(a) Bending (b) Twisting

Figure 6. Modal shapes.

2. STRAINS AND STRESSES ANALYSIS

2.1 Non cavitating flow

Concerning strains' measurements, the experiment was performed from $-10°$ to $10°$ and with a step $\Delta\alpha = 0.5°$, at flow velocity $\mathrm{U} = 5\mathrm{m.s^{-1}}$. The values of ε_i are recorded during 10 seconds and the mean value is computed. In order to study the strains resulted from the flow only, the values in still water are removed. Then, as the hydrofoil section is symmetrical, the strains are null for $\alpha = 0°$. This allows us to adjust precisely the value of the incidence α_0 during the experiments.

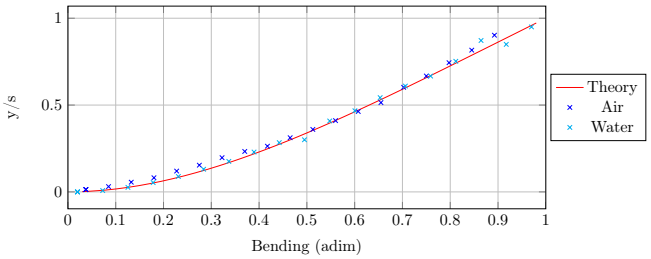

Figure 7. Comparison of the theoretical and experimental modal shapes - bending.

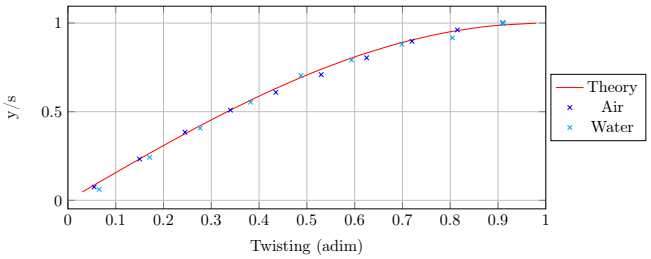

Figure 8. Comparison of the theoretical and experimental modal shapes - twisting.

The results are shown on Figure 9. Again it is observed that the hydrofoil behaves like a built-in beam: ε_1 and ε_2 increase with the angle of attack. The higher strain is ε_1, which corresponds to the span direction (blue line on Figure 9). It is due to the hydrodynamic lift force. The strain ε_3, in the chord direction (green line), is opposed to the others because of the twist and the shearing stress.

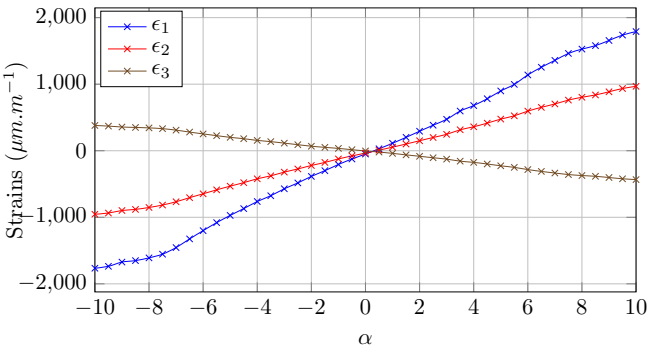

Figure 9. Strains (μm/m) depending on the AoA, $U = 5\mathrm{m.s^{-1}}$.

It is observed that the strains are linear up to 3°. Then they discard from the linear trend. This is particularly true for ε_1 that is highly related to the lift. Figure 10 shows the principal stresses (2) and the Von Mises stresses (3). As shown, an inversion of the principal

stresses' curves appears passing through 0°. This is due to a change of the principal directions. The Von Mises stress is symmetrical and it is linear up to 4° (respectively −4° for negative angle of incidence). Beyond 4° or −4° it discards from the linear evolution.This is a consequence of the lift force evolution that was found to evolve in the same way as a result of boundary layer transition due to a Laminar Separation Bubble at a moderate chord length Reynolds number [22]. It was observed that triggering the boundary layer at the leading edge suppress this peculiar nonlinear behavior.

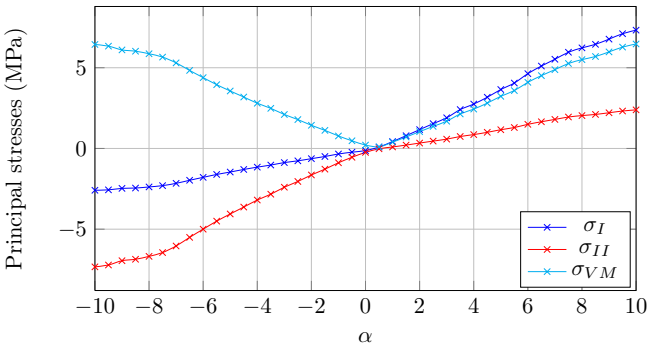

Figure 10. Stresses (MPa) depending on the AoA, $U = 5\text{m.s}^{-1}$.

2.2 Cavitating flows

Measurements have been carried out with a decreasing number of cavitation in order to analyze the behavior of the strains and stresses in cavitating flows. It was observed that depending on the strain direction the mean values of the strains ε_i increases with σ (see ε_1), and decreases for the lowest cavitation number as it is illustrated on Figure 11. In the same time, the strain fluctuations increase as shown by the vertical bars, determined by the standard deviation. This is particularly true for ε_1 directly related to the lift forces. The same observation is clearly shown on the Von Mises stress evolution as function of the cavitation number (Figure 12). As an interesting result, it is shown that strain gauges' response can be a very interesting way to get information on forces acting on the structures. It could be a good way for control lifting surfaces in operating condition.

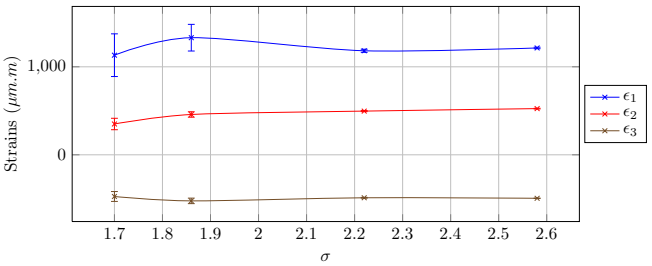

Figure 11. Mean ε_i depending on σ. Vertical bars are determined by the standard deviation.

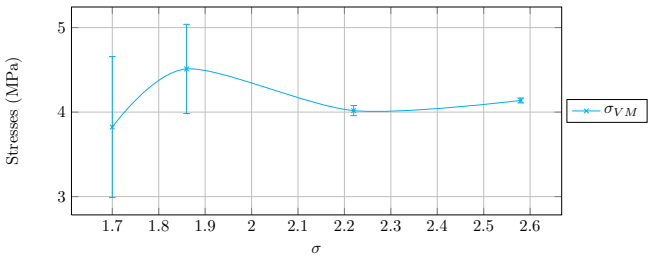

Figure 12. Mean values of Von Mises stress depending on cavitation. Vertical bars are determined by standard deviation.

In fact as the cavitation number decreases, the strain signals experience large fluctuations at a frequency related to the oscillation of the cavity. The frequency, named f_c, decreases as the cavity increases. This is clearly shown on Figure 13, which represents the time series of the Von Mises stresses depending on the cavitation number. It is particularly clear on the Von Mises stresses' signal for $\sigma = 1.70$ (Figure 13). The frequencies of the strain gauge's signals were found to be similar to the vibration's frequencies of the foil reported in the next session.

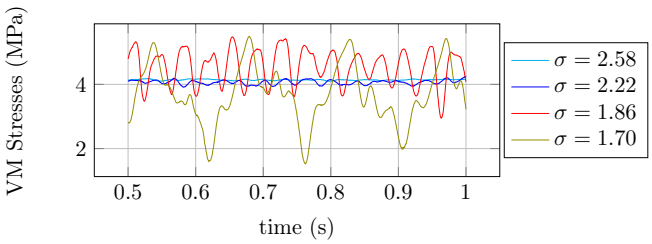

Figure 13. Time-history of Von Mises stresses for different cavitation numbers.

3. FOIL'S VIBRATION

3.1 Non cavitating flows

Measurements were carried out at a constant pressure in the tunnel section close to the atmospheric pressure, for which cavitation does not develop. They were performed for angles of incidence from 0° to 8° with a step $\Delta\alpha = 2°$, the flow velocity was 3, 4, 5 and 6 m.s^{-1}, corresponding to Reynolds numbers based on the chord length ranging from 3.10^5 to 6.10^5. The frequencies of the first two modes, which correspond to bending and twisting modes, are reported on Table 3 for each incidence and each flow velocity. An example of vibration spectra is given on Figure 14, which represents the spectra with $\alpha = 8°$ depending on the flow velocity.

The first mode's frequency (bending) is constant with the flow speed and the angle of attack, whereas the second (twisting) and the third one's increase with the flow speed (Figure 14). For the lowest incidences (0 to 4°) and low flow velocity (3m.s^{-1}), a high peak appears near

Table 3. First two modes frequencies (Hz) depending on the flow speed and the AoA

	$3m.s^{-1}$	$4m.s^{-1}$	$5m.s^{-1}$	$6m.s^{-1}$
8°	36.5 Hz 182 Hz	35.5 Hz 188.5 Hz	37 Hz 191 Hz	37 Hz 194 Hz
6°	37 Hz 185 Hz	36.5 Hz 189.5 Hz	37 Hz 190.5 Hz	36.5 Hz 190.5 Hz
4°	37.5 Hz 187 Hz	35.5 Hz 187.5 Hz	36.5 Hz 187 Hz	36 Hz 189 Hz
2°	36.5 Hz 186.5 Hz	37.5 Hz 187 Hz	37 Hz 186.5 Hz	37 Hz 189.5 Hz
0°	35 Hz 186 Hz	37 Hz 186.5 Hz	36 Hz 190 Hz	37 Hz 184.5 Hz

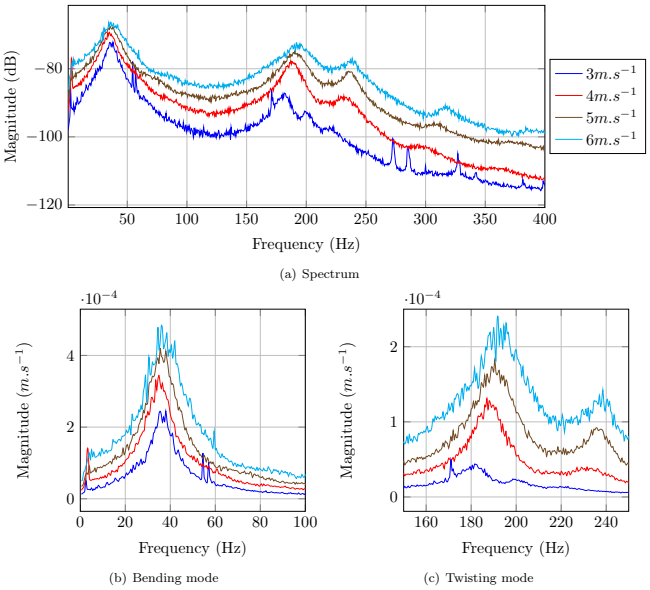

Figure 14. Spectra with $\alpha = 8°$, U = 3 to 6 m.s^{-1} at atmospheric pressure (non cavitating flow).

the twisting mode's frequency (Figure 15). As mentioned previously it is a consequence of the unsteadiness of the Laminar Separation Bubble (LSB) inducing transition at low angle of attack and moderate flow velocities developping on the rear part of the suction side ([23]). This peak disappear when the incidence or the velocity increases. It is explained by the sudden displacement of the LSB and transition towards the leading edge [22].

3.2 Cavitating flows

To study the behavior of the flexible foil with cavitation, measurements have been carried out by decreasing the pressure. The cavitation number is defined by

$$\sigma = \frac{(P_0 - P_v)}{0.5\rho U^2} \tag{4}$$

where P_0 is the pressure at middle of the test section, P_v the vapor pressure at the water temperature, U the

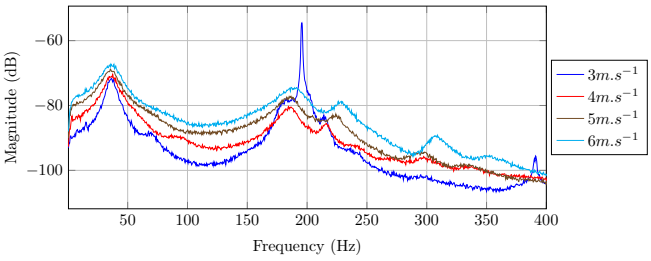

Figure 15. Spectra with $\alpha = 2°$, U = 3 to 6 m.s^{-1} at atmospheric pressure (non cavitating flow).

flow velocity and ρ the water density. The cavitation was controlled by decreasing or increasing the pressure P_0 at a fixed velocity.

Tests have been performed with a fixed flow velocity (U = 6 m.s^{-1}) and two angles of attack ($\alpha = 8, 10°$). For α equal to 8°, eight measurements have been performed, that corresponds to cavitation numbers ranging between $\sigma = 1.52$ and $\sigma = 5.68$ (wetted flow). For α equal to 10°, six measurements have been carried out with σ decreasing from 2.51 to 1.52. The spectra are shown on Figure 16 and Figure 17.

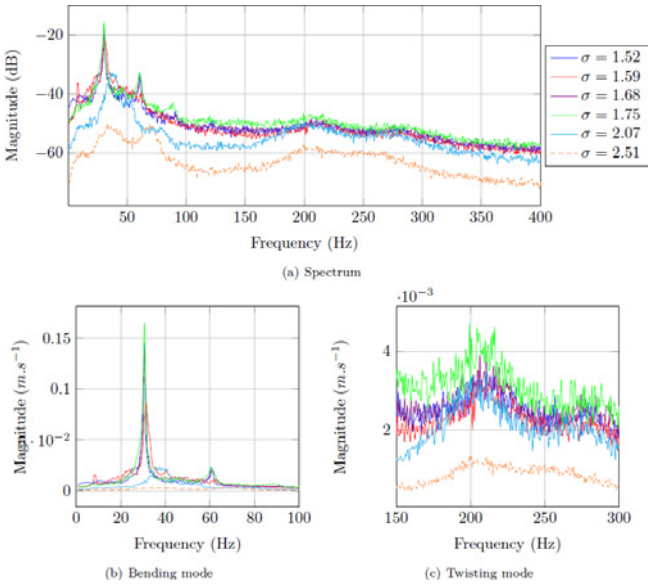

Figure 16. Response of a foil in cavitating flow, $\alpha = 10°$, U = 6m.s^{-1}.

As shown on Figure 17, the frequencies of the twisting and the third modes increase as σ decreases. On the contrary, even it is not very significant, the bending mode's frequency tends to decrease slightly as the cavitation develops. For the lowest cavitation numbers (σ lower than 1.41), a low frequency peak and its harmonics appear. For $\alpha = 8°$, the first peak corresponds to the bending mode's frequency and is constant until $\sigma = 1.6$, then it falls to 8Hz. The same trend is visible on the curves with $\alpha = 10°$, but the fall seems to occur later.

To study more deeply this phenomenon, high speed

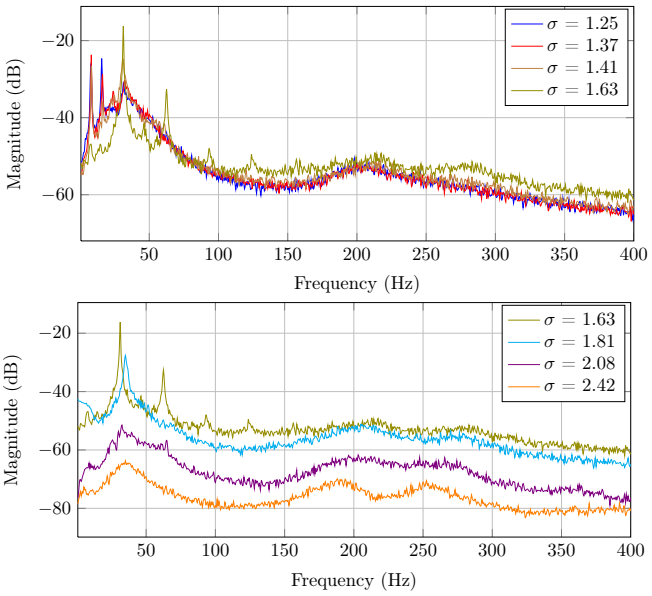

Figure 17. Vibration spectra in cavitating flow, $\alpha = 8°$, U = 6m.s^{-1} (Spectra are displayed on two subfigures (a) and (b) depending on σ to improve visibility, the green curve ($\sigma = 1.63$) is represented on both figures)

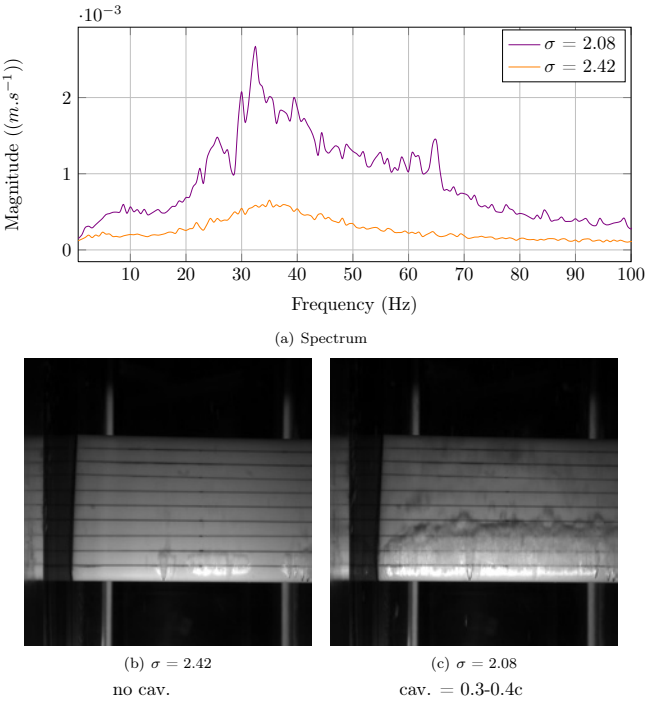

Figure 18. Vibration spectra in cavitating flow, $\alpha = 8°$, U = 6m.s^{-1} (Spectra are displayed on two subfigures (a) and (b) depending on σ to improve visibility, the green curve ($\sigma = 1.63$) is represented on both figures)

movies was recorded to observe the cavitating flow developing on the suction side. It was observed that for α equal to 8° and $\sigma = 2.42$, attached bubbles appear on the foil mainly due to surface irregularities (Figure 18). As the pressure decrease, a sheet cavitation attached to the leading edge takes places and oscillate between 20 and 50% of the chord for $\sigma = 2.08$. In that case, the frequency of cavity oscillation is close to the bending mode's frequency of the foil that implies a lock-in between both frequencies and a strong increase of the magnitude of the peak. A second peak corresponding to the harmonic of the cavity oscillation is observed as cavitation develops more.

For $\sigma = 1.81$ and 1.63 (Figure 19), the cavity oscillation amplitude becomes very large. The cavity oscillates from 0% to 70% of the chord length before being carried away downstream. The frequency of the cavity oscillation, noted f_o, can be deduced from the high speed camera records between two periods of the cavity evolution. The frequencies correspond to the higher peaks of the frequency vibration responses, that explains the decrease of the first peak's frequency from the bending mode frequency (around 34.4Hz) to 30Hz. Harmonics of this frequency are observed for $\sigma = 1.63$.

As the cavitation number becomes lower than $\sigma = 1.41$, a peak appears at f = 8Hz (Figure 20) and subsequent harmonics are observed. This low frequency peak corresponds to the oscillation frequency of the cavity. In that case the vapor cavity oscillates from fully wetted to nearly 100% of the chord length. Its higher order harmonics are relatively low but can interact with the bending 30Hz-peak. As the pressure decreases again ($\sigma = 1.37$ and 1.25), this interaction disappears and the first harmonic becomes stronger.

The Table 4 gathers the oscillation frequencies f_o obtained from high speed visualization and the main frequencies of the foil vibration spectrum, called f_m, according the cavitation number.

Table 4. Oscillation frequencies of the cavity sheet and main frequencies of the foil depending on the cavitation number, $\alpha = 8°$, U = 6m.s^{-1}.

σ	2.42	2.08	1.81	1.63	1.41	1.37	1.25
f_o	-	-	33	31.4	8.51	8.54	7.84
f_m	35	35	35	31	8	8	8

The same phenomenon is observed with $\alpha = 10°$. For $\sigma = 2.51$ and $\sigma = 2.07$, a sheet cavitation oscillates between 20% and 40%, and between 0 and 50% respectively, but no frequency appears distinctly on the films. Then we can observe a growth of the cavity until the shedding with a measurable frequency value of approximately 30.3Hz for $\sigma = 1.75$ and 33Hz for $\sigma = 1.59$, very close to bending frequency.

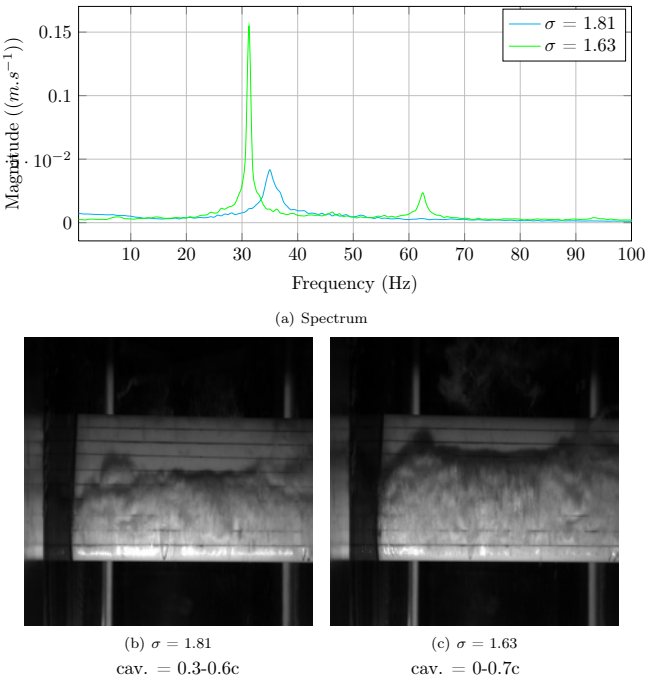

Figure 19. Vibration spectra in cavitating flow, $\alpha = 8°$, $U = 6 m.s^{-1}$ (Spectra are displayed on two subfigures (a) and (b) depending on σ to improve visibility, the green curve ($\sigma = 1.63$) is represented on both figures)

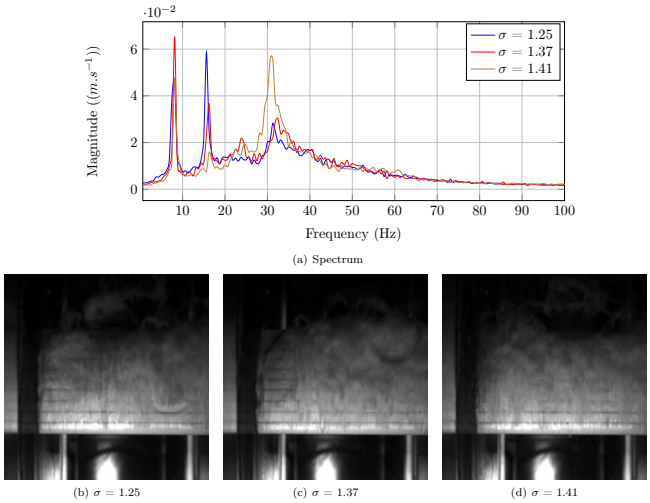

Figure 20. Vibration spectra in cavitating flow, $\alpha = 8°$, $U = 6 m.s^{-1}$ (Spectra are displayed on two subfigures (a) and (b) depending on σ to improve visibility, the green curve ($\sigma = 1.63$) is represented on both figures)

4. CONCLUSION

An original experimental procedure was developed to analyze Fluid Structure Interaction on flexible lightweight lifting structures operating in heavy fluid and cavitating flow. Specific hydrofoils were constructed in order to measure the static deformation, the strains, the stresses and the vibrations of a rectangular cantilevered flexible NACA 0015 section hydrofoil made of POM, in sub-cavitating flow and in unsteady partial cavitation flow. The experiments were performed in the cavitation tunnel of the French Naval Academy. The hydrofoil was equipped with strain gauges embedded close to the root of the foil. Vibrations measurements were carried out using vibrometers. Many new observations can be reported. It was observed that the cantilevered rectangular hydrofoil has a beam-like behavior with bending and twisting deformation mainly. The strains evolve linearly with the angle of incidence as the hydrodynamic loading. In partial cavitating flow, the average value of the strains and stresses tend to increase in the first stage of cavitation together with an increase of fluctuations. As the vapor cavity increased again, the strains and stresses felt down together with a strong increase of fluctuations. This was clearly observable on the Von-Mises stress measurement. Concerning vibrations, the bending and twisting mode's frequencies were clearly identified thanks to impulse tests on the foil's surface in the air and in still water. The effect of added-mass in heavy fluid is clearly determined by a net decrease of the modal frequencies. Then measurements in non cavitating flow were performed for various flow velocities corresponding to Reynolds number ranging from 3.10^5 to 6.10^5, and various angle of attack (AoA) from 0° to 8°. It is observed that the bending mode's frequency is constant as the AoA or the flow velocity increases. On the other hand, the twisting and the third mode's frequencies tend to increase with the flow velocity and incidence. A peculiar vibration phenomenon was observed at relatively low AoA. It induced a strong peak at a given frequency that can be related to a laminar separation bubble and boundary layer transition. It was observed that the phenomenon disappears as the AoA or the velocity increases or by triggering the boundary layer close to the leading edge.

The measurements carried out in unsteady cavitating flow allowed us to notice that the bending mode's frequency changes slightly depending on the oscillation frequency of the cavity, resulting from a frequency lock-in with the cavity oscillation's frequency and harmonics or subharmonics . Moreover, the twisting mode's frequency tends to increase with the cavity length that could be related to a decrease of the added mass effects in presence of a vapor cavity on the foil surface.

This work brings new informations about the physics of FSI on lightweight flexible structures in a heavy fluid that should be very interesting for physical analysis and simulation of relative complex flow in FSI. This work has to be followed with different enhancements. In particular, some observations need to be studied more deeply. The hydrodynamic force measurements on flexible foil should be also examined. Moreover, tests should be performed with other foils made of other flexible materials.

ACKNOWLEDGMENTS

The authors wish to acknowledge the Office of Naval Research for the support under the grant number N62909-12-1-7076, as well as the technical staff of the Naval Academy Research Institute, Alain Boulch is gratefully acknowledged.

REFERENCES

[1] C. E. Brennen. Cavitation and bubble dynamics. *Oxford University Press*, 1995.

[2] J. P. Franc. Physics and control of cavitation. *Design and analysis of high speed pumps*, 2:1–36, 2006.

[3] J. A. Astolfi, J. B. Leroux, P. Dorange, J. Y. Billard, F. Deniset, and S. De La Fuente. An experimental investigation of cavitation inception and development on a two-dimensional hydrofoil. *Journal of ship research*, 44:259–269, 2000.

[4] J. B. Leroux, O. Coutier-Delgosha, and J. A. Astolfi. A joint experimental and numerical study of mechanisms associated to instability of partial cavitation on two-dimensional hydrofoil. *Physics of Fluids*, 5:52–101, 2005.

[5] Y. L. Young. Fluid–structure interaction analysis of flexible composite marine propellers. *Journal of Fluids and Structures*, 24:799–818, 2008.

[6] T. Sontvedt. Propeller blade stresses, application of finite element methods. *Computers and Structures*, 4:193–204, 1974.

[7] H. J. Lin, J. J. Lin, and T. J. Chuang. Strength evaluation of a composite marine propeller blade. *Journal of Reinforced Plastics and Composites*, 24:1791–1807, 2005.

[8] Y. L. Young. Hydroelastic behavior of flexible composite propellers in wake inflow. *Proc. of 16th International Conference on composite materials, Kyoto, Japan*, 2007.

[9] Y. L. Young, M. R. Motley, and R. W. Yeung. Hydroelastic response of wind or tidal turbines. *Proc. of 28th International Conference on Ocean, Offshore and Arctic Engineering, Honolulu, USA,*, pages 101–110, 2009.

[10] N. L. Mulcahy, B. G. Prusty, and C. P. Gardiner. Flexible composite hydrofoils and propeller blades. *Proc. of International Maritime Conference 2010: Maritime Industry - Challenges, Opportunities and Imperatives, Sydney, Australia*, pages 438–448, 2010.

[11] M. R. Motley and Y. L. Young. Performance-based design and analysis of flexible composite propulsors. *Journal of Fluids and Structures*, 27:1310–1325, 2011.

[12] O. Coutier-Delgosha, B. Stutz, A. Vabre, and S. Legoupil. Analysis of cavitating flow structure by experimental and numerical investigations. *Journal of Fluid Mechanics*, 578:171–222, 2007.

[13] P. Ausoni, M. Farhat, X. Escaler, E. Egusquiza, and F. Avellan. Cavitation influence on von karman vortex shedding and induced hydrofoil vibrations. *Journal of Fluids Engineering*, 129:966, 2007.

[14] A. Ducoin, F. Deniset, J. A. Astolfi, and J.-F. Sigrist. Numerical and experimental investigation of hydrodynamic characteristics of deformable hydrofoils. *Journal of Ship Research*, 53:214–226, 2009.

[15] M. C. Reese. Vibration and damping of hydrofoil in uniform flow. *Thesis, Pennsylvania State University*, 2010.

[16] A. Ducoin, J. A. Astolfi, and J.-F. Sigrist. An experimental analysis of fluid structure interaction on a flexible hydrofoil in various flow regimes including cavitating flow. *European Journal of Mechanics/B*, 36:63–74, 2012.

[17] F. Gaugain, F. Deniset, J. A. Astolfi, and J.-F. Sigrist. Numerical and experimental study of hydroelastic behaviour of a hydrofoil. *Proc. of 10th International Conference on Flow-Induced Vibrations, Dublin*, pages 67–74, 2012.

[18] D. T. Akcabay and Y. L. Young. Influence of cavitation on the hydroelastic stability of hydrofoils. *Journal of Fluids and Structures*, 49:170–185, 2014.

[19] D. T. Akcabay, E. J. Chae, Y. L. Young, A. Ducoin, and J. A. Astolfi. Cavity induced vibration of flexible hydrofoils. *Journal of Fluids and Structures*, 49:463–484, 2014.

[20] M. Benaouicha, J. A. Astolfi, A. Ducoin, S. Frikha, and O. Coutier-Delgosha. A numerical study of cavitation induced vibration. *Proc. of Pressure Vessels and Piping Conference, Washington, USA*, 2010.

[21] M. Benaouicha and J. A. Astolfi. Analysis of added mass in cavitating flow. *Journal of fluids and structures*, 31:30–48, 2012.

[22] P. L. Delafin, F. Deniset, and J. A. Astolfi. Effects of the laminar separation bubble induced transition on the hydrodynamic performance of a hydrofoil. *European Journal of Mechanics/B*, 46:190–200, 2014.

[23] A. Ducoin, J. A. Astolfi, and M. L. Gobert. An experimental study of boundary layer transition induced vibrations on a hydrofoil. *Journal of Fluids and Structures*, 32:37–51, 2012.